Magnetic field imaging of a tungsten-carbide film by scanning nano-SQUID microscope

Yusuke Shibata and Shintaro Nomura*

Division of Physics, University of Tsukuba,

Tennodai, Tsukuba, 305-8571, Japan

Ryosuke Ishiguro

Center for Emergent Matter Science, RIKEN,

2-1 Hirosawa, Wako, Saitama 351-0198,

Japan and Department of Mathematical and Physical Sciences,

Faculty of Science, Japan Women's University,

Mejirodai, Bunkyo-ku, Tokyo 112-8681, Japan

Hiromi Kashiwaya and Satoshi Kashiwaya

National Institute of Advanced Industrial Science and Technology (AIST),

Umezono, Tsukuba, 305-8568, Japan

Yusuke Nago and Hideaki Takayanagi

Department of Applied Physics, Faculty of Science,

Tokyo University of Science, Tokyo 125-8585, Japan

(Dated: July 15, 2016)

Abstract

We present results of magnetic field imaging by scanning nano-superconducting quantum interference device (SQUID) microscopy on a tungsten-carbide (W-C) film fabricated using focused-ion-beam chemical vapor deposition. We have investigated magnetic field change by a W-C film in an external magnetic field using a scanning nano-SQUID microscope system. We have found that the reduction of magnetic field above the W-C film was 0.9%, indicating penetration of vortices in the W-C at an external magnetic field of 0.171 mT.

---
*nomura.shintaro.ge@u.tsukuba.ac.jp

I. INTRODUCTION

Focused-ion-beam chemical vapor deposition (FIB-CVD) [1–3] with Ga^+ beam and tungsten hexacarboxyl $(W(CO)_6)$ precursor [4, 5] is a promising technique to prepare superconducting films. FIB-CVD deposition of superconducting films has been acquired much interest as a template-free method to fabricate nano-superconducting quantum interference devices (SQUIDs) that enables precise control of deposition, for example, at the apex of a probe tip of a scanning nano-SQUID microscope. A superconductor/normal metal/superconductor Josephson junction was fabricated using FIB-CVD and Fraunhofer oscillation of the critical current was observed [6]. FIB-CVD also provides a method to repair or modify superconducting circuits [7].

Thin films prepared by FIB-CVD of $W(CO)_6$ are amorphous with typical atomic concentrations of W: C: Ga = 40%: 40%: 20%, [4, 5] and are often called as tungsten-carbide (W-C) films. W-C nanowires were reported to exhibit superconductivity at a critical temperature T_c of 5.2 K [4], which is much higher than the critical temperature of bulk crystalline tungsten of 0.01 K [8]. High T_c of W-C nanowires is associated with their amorphous structure [4, 9]. It has been shown that T_c of W-C wires was fitted well by a theory as a function of a parameter for the level of disorders [10, 11]. Superconductivity of W-C nanowires critically depends on the concentration of W. It was reported that W-C nanowires were superconducting for W concentration between 17.5 and 40% [11]. A tunneling spectroscopy measurement indicates that a W-C film has a superconducting gap of $\Delta = 0.66$ meV following s-wave BCS theory [12], while the melting transition in a vortex lattice was observed below T_c by scanning tunneling spectroscopy. [13] The current-voltage properties of W-C strips in high magnetic fields were reported to follow the quasi-three-dimensional vortex glass to liquid transition theory [14].

FIB-CVD deposition of W-C films is a promising method for fabrications of nanometer-size Josephson junctions and nano-SQUIDs [15]. For this purpose, investigations of diamagnetic and superconductivity properties of W-C films are important. We employ a Nb weak-link scanning nano-SQUID microscope [16] to explore superconducting properties of a W-C film. SQUIDs have been recognized to be the most sensitive magnetic field and flux detectors [17–21]. Efforts have recently been made to reduce the size of the SQUID loop to explore properties of nanoscale objects with high spatial resolution [16, 22–25]. Reduction

2

in the size of the SQUID loop allows strong coupling of the SQUID loop to the sample nanoscale object, leading to higher spatial resolution and sensitivities. Moreover, the limiting flux noise spectral density decreases with reduction in the size of the SQUID loop [18] and the magnetic moment sensitivity is approaching single Bohr magneton μ_B [24]. Recently, we have developed a nano-SQUID microscope based on weak-link Josephson junctions with sufficiently-small hysteresis that enables the SQUID to be operated as a magnetic flux to voltage transducer [16]. In this paper, we investigate magnetic field distribution in the vicinity of a W-C film in an external magnetic field by our Nb weak-link scanning nano-SQUID microscope.

II. METHODS

We used a dual-beam FIB-scanning electron microscope system (NB5000, Hitachi High-Technologies) to deposit W-C films. The acceleration voltage of Ga$^+$ ion beam was 40 kV and the base pressure was 1×10^{-4} Pa. We used tungsten hexacarboxyl (W(CO)$_6$) precursor. W-C films with thickness of 300 nm were grown with Ga$^+$ ion beam current of 700 pA at 1×10^{-3} Pa on a p-Si substrate. Nb/Au electrodes were fabricated by electron beam lithography with thicknesses of Nb and Au of 600 and 30 nm, respectively. Figure 1 shows an optical micrograph of a deposited square W-C film with the size of 20 μm $\times$ 20 μm. On the left side of the square W-C film, two Nb/Au wires with a width of 2 μm were deposited. In the vicinity of the W-C film, a yellow blurred region is seen in figure 1, due to unintentional deposition of W-C by the scatterings of ion beams. A W-C strip with the size of 60 μm $\times$ 4 μm was prepared for four-terminal electric transport measurements.

We used a home-built scanning nano-SQUID microscope system to measure real-space imaging of magnetic field [16]. A Dayem Nb nano-SQUID probe with a loop size of 1 μm and a nano-bridge width of 80 nm was attached to a quartz tuning fork for a feed-back control of the distance between the sample surface and the SQUID probe. The nano-SQUID probe faced $\theta = 51°$ to the surface of the sample, and detected magnetic field of $B_M(x, y, z) = B_y(x, y, z)\sin\theta + B_z(x, y, z)\cos\theta$. The sample W-C film was scanned using closed loop inertially-actuated triaxial stepping piezoelectric-stages with resistive position encoders in a cryogen-free pulse tube refrigerator (Optistat PT, Oxford Instruments) with base temperature of 3.4 K. Typical minimum step size was 10 nm in the coarse positioning

3

mode. Scanning measurements were performed at a constant height mode by monitoring the resistive position encoder. Perpendicular magnetic field to the sample surface was applied using a home-made superconducting magnet with the bore size of 50 mm. Details of the scanning nano-SQUID system can be found elsewhere [16]. Electric transport measurements were performed by using a physical property measurement system (PPMS, Quantum Design).
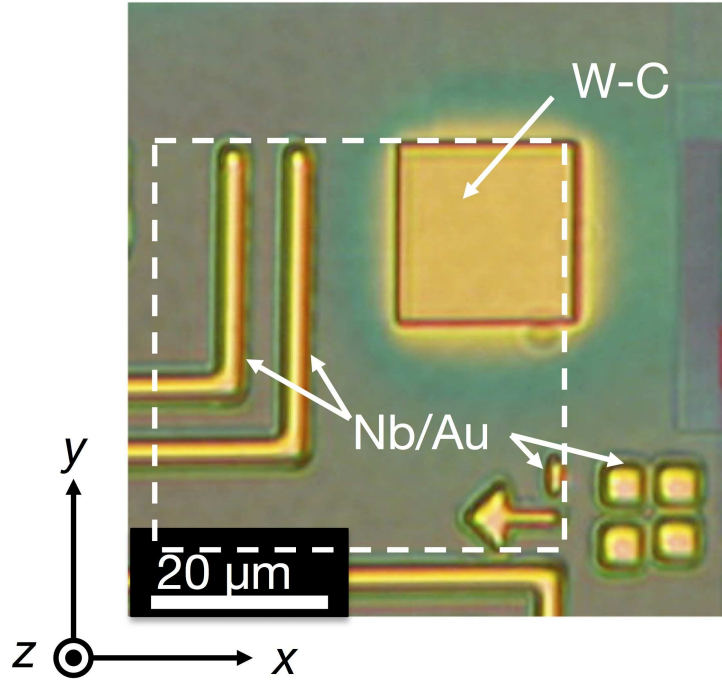

FIG. 1. Optical micropraph of an FIB assisted tungsten carbide film. The thickness and the size of the tungsten carbide film was 300 nm and 20 μm × 20 μm, respectively. Two niobium wires are seen on the left part of the optical micrograph. Dashed white box indicates the displayed area of 45 μm × 45 μm in figure 3(a).
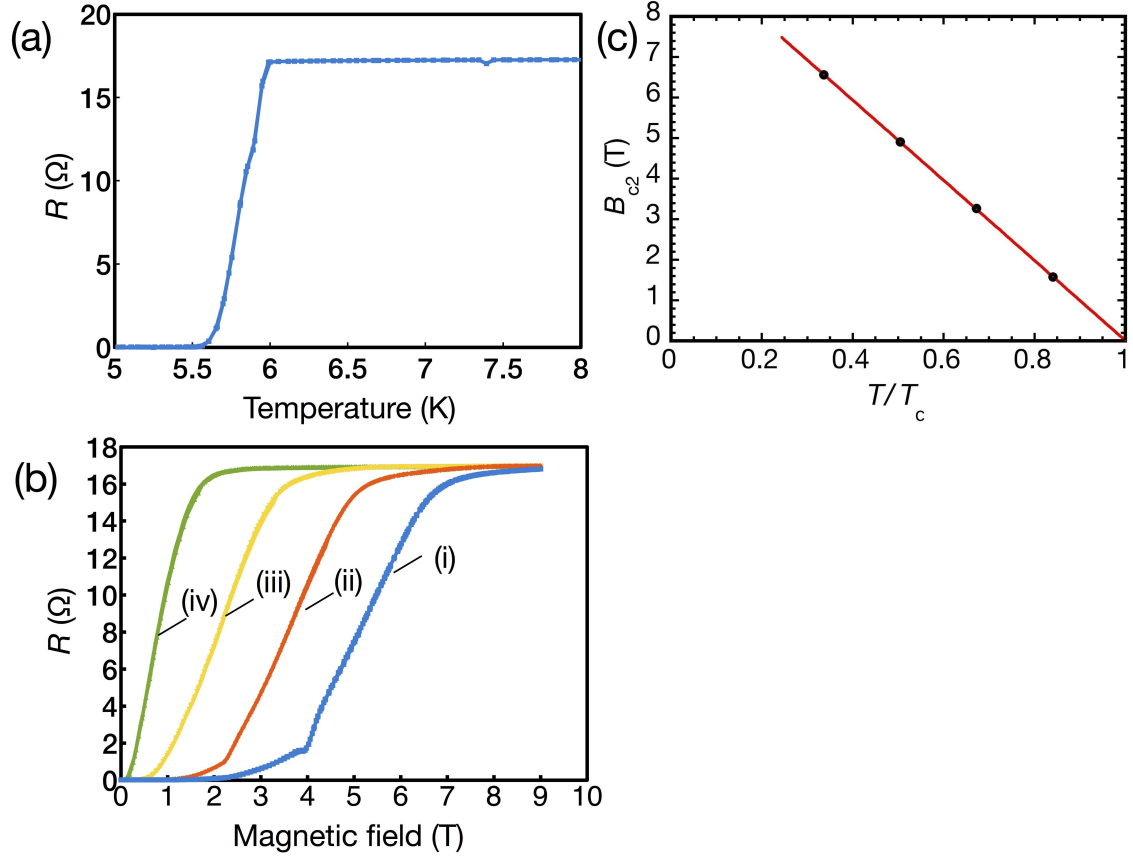
FIG. 2. (a) Temperature dependence of resistance of tungsten-carbide wire at 0 T. (b) Perpendicular magnetic field dependence of resistance of tungsten wire at (i) 2.0, (ii) 3.0, (iii) 4.0 and (iv) 5.0 K. (c) Upper critical field B_{c2} as a function of T/T_c. The red line is the best fitted line to Eq. (1).

III.   RESULTS AND DISCUSSION

A.   Characterizations of W-C film

An optical micrograph of a W-C film is shown in figure 1. The deposited W-C is seen to spread about several μm outside of the designed pattern of a square of 20 μm $\times$ 20 μm. This contrasts with the sharp edges of Nb/Au wires fabricated by EB lithography as seen in the left of the square W-C in figure 1. Temperature dependence of the four-terminal resistance (R) of the W-C wire sample with a width of 4 μm is shown in figure 2 (a) at an excitation current of 10 μA at 0 T. Figure 2(a) indicates that the W-C sample is zero resistance below 5.5 K. The superconducting transition temperature T_{c} as defined by 10% of resistance drop from the resistance at the normal phase R_{n} ($R/R_{\mathrm{n}} = 0.9$) is 5.9 K, which is comparable to the reported values of $T_{\mathrm{c}} = 4.8$-6.2 K for W-C samples fabricated by FIB deposition [4, 5, 11, 12, 14]. The critical current density was estimated to be $J_c = 1.3 \times 10^6$ and 2.1×10^5 A/cm^2 at 2.0 and 4.0 K, respectively, which is slightly larger than the reported value for thin film of 1.5×10^5 A/cm^2 at 3 K [4] probably because of differences in the film thickness and the growth condition.

Figure 2(b) shows perpendicular magnetic field dependence of resistance of the W-C wire sample at 2.0-5.0 K. The upper critical field $B_{\mathrm{c}2}$ is plotted in figure 2(c) as a function of T/T_{c}. The Ginzburg-Landau coherence length [26] is estimated to be $\xi_{\mathrm{GL}}(0) = 5.8$ nm by using

$$B_{\mathrm{c}2} = \frac{\Phi_0}{2\pi\xi_{\mathrm{GL}}(0)^2} \left(1 - \frac{T}{T_c}\right),\tag{1}$$

where Φ_0 is the magnetic flux quantum.

B.   Mapping of magnetic field change by W-C film

The scanning nano-SQUID microscopy was performed at a constant height mode with the distance between the SQUID probe and the sample surface of 3.5 μm. The scanning direction was parallel to the y-axis. Mapping of magnetic field normalized by magnetic field of 0.171 mT is shown in figure 3(a). Reduction of magnetic field due to Meissnner effect of the superconducting niobium wire with a width of about 2 μm is clearly seen, however, the reduction of magnetic field on the square W-C film of 20 μm $\times$ 20 μm is small as shown in

figure 3(a). A line profile of magnetic field change in figure 3(b) shows reduction of magnetic field due to niobium wires in the region $-17 < x < -13$ μm and at $-11 < x < -7$ μm. Reduction of magnetic field due to the W-C film was 0.9%.

C. Calculation of magnetic field distribution by a finite element method

Magnetic field distributions around Nb and W-C films were calculated by numerically solving Maxwell's and London equations using a finite element method with a commercial package, COMSOL. Nb wires with 2 μm $\times$ 20 μm $\times$ 0.6 μm and a W-C film with 20 μm $\times$
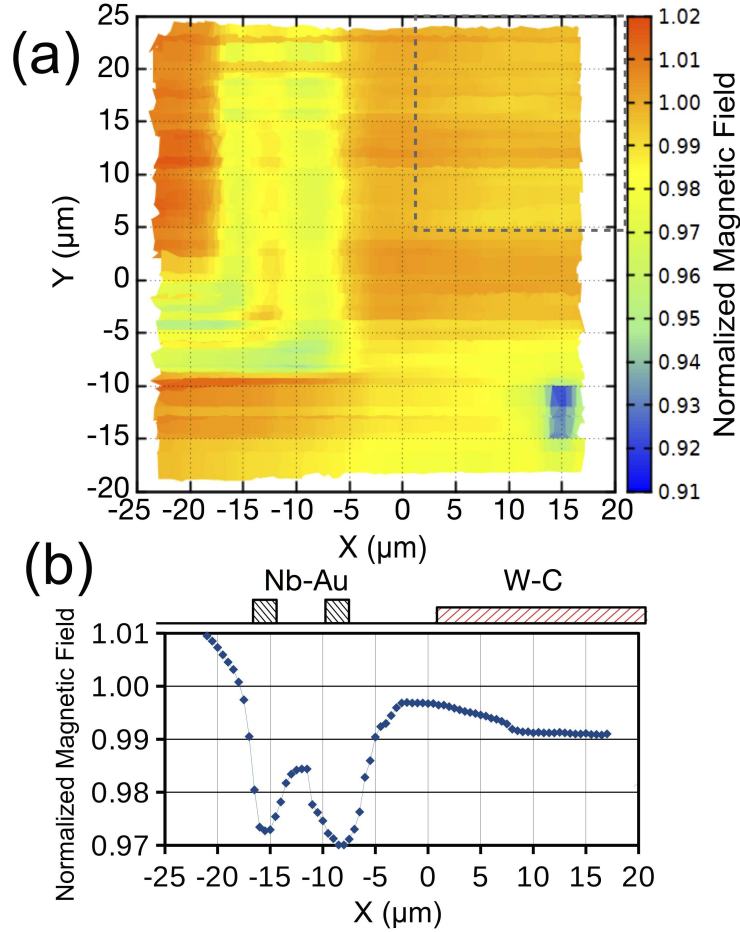

FIG. 3. (a) Mapping of magnetic field normalized by magnetic field of 0.171 mT at (x, y)=(0 μm, 0 μm). The dashed square indicates the position of the tungsten carbide film. (b) A lineprofile of normalized magnetic field averaged at $6 \leq y \leq 10$ μm. The hatched squares on top of the panel indicate the positions of Nb/Au and W-C films.

20 μm $\times$ 0.3 μm were modelled in the calculation. London equation $\Delta\mathbf{B} = \mathbf{B}/\lambda_{\text{eff}}^2$ was solved inside the Nb wires and the W-C film and Laplace's equation $\Delta\mathbf{B} = 0$ was solved elsewhere. The effective London penetration depth λ_{eff} for Nb wires was fixed to be 1 μm, and λ_{eff} for a W-C film was varied between 0.85 and 1.6 μm. Numerical calculations were performed using 1,167,697 domain elements, generated by COMSOL for 3-dimensional region of $80 \times 60 \times 16$ μm^3 as shown in figure 4. The sizes of the elements around the Nb wires and the W-C film were approximately 0.042 and 0.17 μm, respectively.

Figures 5(a) and (b) show calculated perpendicular magnetic field distribution (B_z) on the surface of Si substrate and a crosssection at $y = 0$ μm and $z = 3.5$ μm at an external magnetic field of 0.171 mT. Figures 5(a) and (b) indicate that the reduction of the magnetic field is larger in the region above the W-C film than in the region above Nb wires, contradicting with our observations in figure 3. This result suggests that λ_{eff} much larger than 1.6 μm for a W-C film should be assumed to reproduce our result, or alternatively vortices are penetrating through the W-C film. λ_{eff} and $\xi_{\text{GL}}(0)$ for a W-C film with a thickness of 200 nm was estimated to be 850 and 6.25 nm, respectively [13]. It is unlikely to assume λ_{eff} much larger than 1.6 μm because $T_c = 5.9$ K of our sample is larger than $T_c = 4.15$ K in the literature [13]. The external magnetic field of 0.171 mT is strong enough to allow penetration of vortices into the W-C film because we have $\Phi/\Phi_0 = 33.1$, where $\Phi = BA$ is the magnetic flux penetrating an area $A = 20 \times 20$ μm^2. Consequently, we consider the latter is more plausible, and calculated magnetic field distributions around Nb and W-C films by
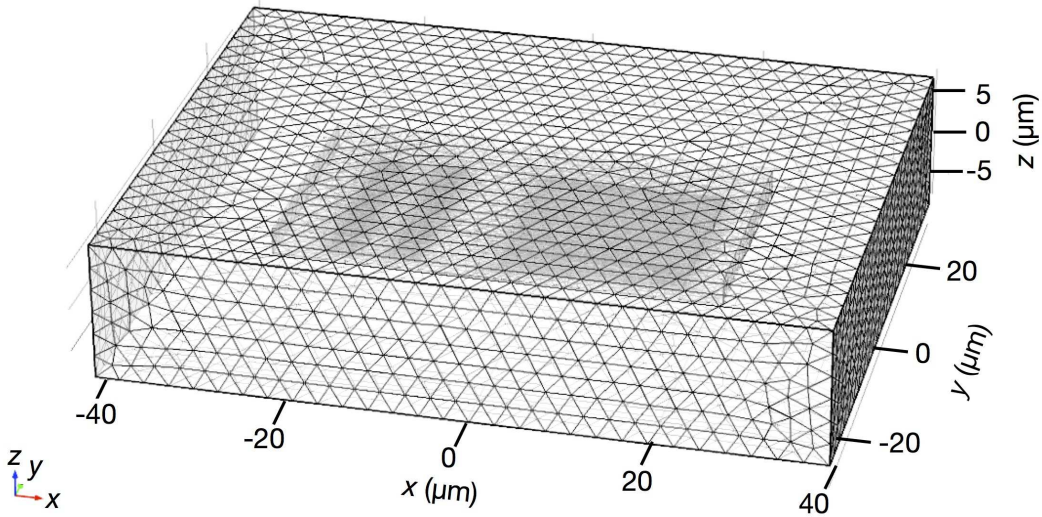

FIG. 4. 3-dimensional meshes for modelling Nb and W-C superconductors.

assuming 9 vortices are present in the square 20 μm $\times$ 20 μm W-C film as shown in figures 5(c) and (d). It has been shown by solving a linearlized Ginzburg-Landau equation [27, 28] that the Ginzburg-Landau free energy is lower for a square lattice of vortices than for a triangular lattice due to the square shape of the W-C film [29]. The lineprofiles in figure 5(d) for $\lambda_{\mathrm{eff}} = 1.4$ μm reproduces smaller reduction of the magnetic field on the W-C film than on the Nb wires. This result qualitatively reproduces our observation overlaid in figure 5 (d).

Guillamon et al. performed low temperature scanning tunneling microscopy (STM) [12, 13] and spectroscopy measurements in W-C thin films, and they observed absence of hexagonal vortex lattice below about 0.2 T, instead they observed bunching of vortices close to linear depressions observed in a topographic STM image. The spacing between linear de-
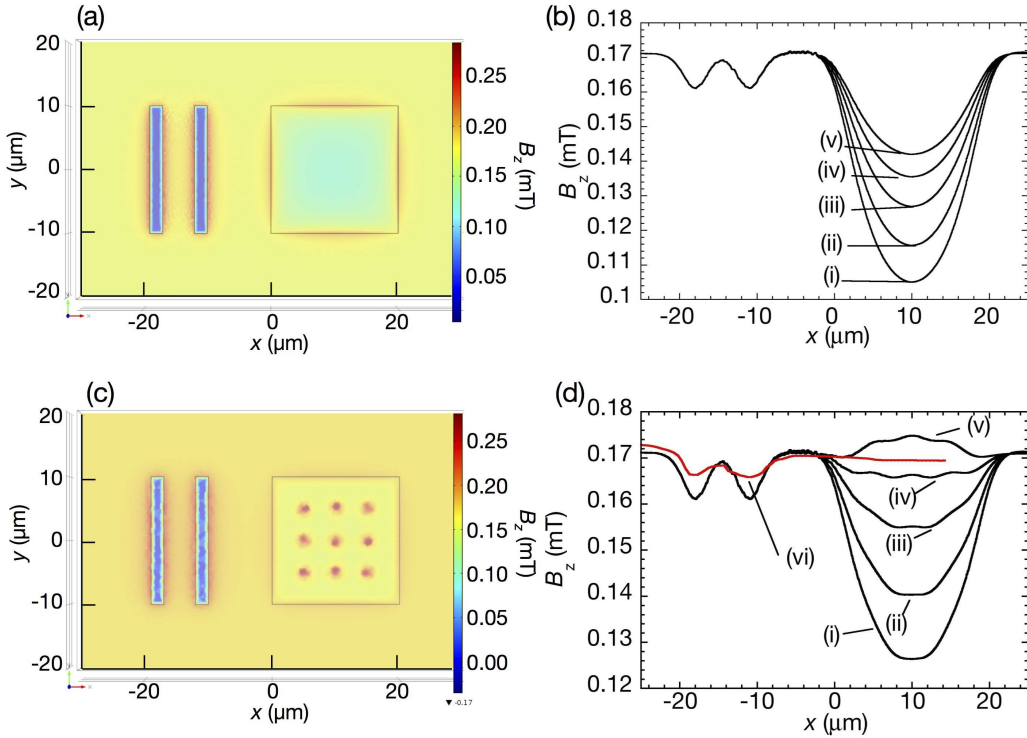

FIG. 5. (a) Calculated perpendicular magnetic field distribution (B_z) on the surface of the sample (z=0 μm). (b) Calculated perpendicular magnetic field distribution at y=0 μm and z=3.5 μm for λ_{eff} = (i) 0.85, (ii) 1.0, (iii) 1.2, (iv) 1.4, and (v) 1.6 μm. (c) (a) for the case of 9 vortices in the W-C sample. (d) (b) for the case of 9 vortices in the W-C sample. (vi) A line profile of measured magnetic field (red) is also shown.

pressions was 100-300 nm, below the spatial resolution of our SQUID microscope. Moreover, they found that vortices at smooth and very flat regions change their position easily. The incomplete cancellation of the external magnetic field in the W-C film in our measurements is consistent with their observations.

IV.　CONCLUSION

In this paper, reduction of magnetic field on Nb/Au wires and a W-C film has been measured. We have found that the reduction of magnetic field above the W-C film was 0.9%. The numerically calculated magnetic field distribution with vortices penetrating the W-C film qualitatively reproduces the measured magnetic field change. Our results indicate that FIB CVD deposition of superconducting films is a promising template-free method to fabricate superconducting nano-devices such as nano-SQUIDs.

[1] K. Gamo, N. Takakura, N. Samoto, R. Shimizu, and S. Namba, Jpn. J. Appl. Phys. **23**, L293 (1984)

[2] S. Matsui and Y. Ochiai, Nanotechnology **7**, 247 (1996)

[3] I. Utke, P. Hoffmann, and J. Melngailis, J. Vac. Sci. Technol. B **26**, 1197 (2008)

[4] E. S. Sadki, S. Ooi, and K. Hirata, Appl. Phys. Lett. **85**, 6206 (2004)

[5] E. Sadki, S. Ooi, and K. Hirata, Physica C: Superconductivity **426-431**, 547 (2005)

[6] J. Dai, R. Kometani, K. Onomitsu, Y. Krockenberger, H. Yamaguchi, S. Ishihara, and S. Warisawa, J. Micromech. Microeng. **24**, 055015 (2014)

[7] M. J. Martínez-Pérez, J. Sesé, F. Luis, R. Córdoba, D. Drung, T. Schurig, E. Bellido, R. d. Miguel, C. Gómez-Moreno, A. Lostao, and D. Ruíz-Molina, IEEE Trans. Appl. Super. **11**, 345 (2011)

[8] J. W. Gibson and R. A. Hein, Phys. Rev. Lett. **12**, 688 (1964)

[9] I. Luxmoore, I. Ross, A. Cullis, P. Fry, J. Orr, P. Buckle, and J. Jefferson, Thin Solid Films **515**, 6791 (2007)

[10] M. S. Osofsky, R. J. Soulen, J. H. Claassen, G. Trotter, H. Kim, and J. S. Horwitz, Phys. Rev. Lett. **87**, 197004 (2001)

[11] J. Dai, K. Onomitsu, R. Kometani, Y. Krockenberger, H. Yamaguchi, S. Ishihara, and S. Warisawa, Jpn. J. Appl. Phys. **52**, 075001 (2013)

[12] I. Guillamón, H. Suderow, S. Vieira, A. Fernández-Pacheco, J. Sesé, R. Córdoba, J. De Teresa, and M. Ibarra, New J. Phys. **10**, 093005 (2008)

[13] I. Guillamón, H. Suderow, A. Fernandez-Pacheco, J. Sesé, R. Córdoba, J. M. De Teresa, M. R. Ibarra, and S. Vieira, Nat. Phys. **5**, 651 (2009)

[14] Y. Sun, J. Wang, W. Zhao, M. Tian, M. Singh, and M. H. W. Chan, Sci. Rep. **3**, 2307 (2013)

[15] C. Granata and A. Vettoliere, Physics Reports **614**, 1 (2016)

[16] Y. Shibata, S. Nomura, H. Kashiwaya, S. Kashiwaya, R. Ishiguro, and H. Takayanagi, Sci. Rep. **5**, 15097 (2015)

[17] K. Hasselbach, C. Veauvy, and D. Mailly, Physica C **332**, 140 (2000)

[18] J. Gallop, Supercond. Sci. Technol. **16**, 1575 (2003)

[19] M. Faley, K. Pratt, R. Reineman, D. Schurig, S. Gott, C. Atwood, R. Sarwinski, D. Paulson, T. Starr, and R. Fagaly, Supercond. Sci. Technol. **17**, S324 (2004)

[20] M. E. Huber, N. C. Koshnick, H. Bluhm, L. J. Archuleta, T. Azua, P. G. Bjrnsson, B. W. Gardner, S. T. Halloran, E. A. Lucero, and K. A. Moler, Rev. Sci. Instrum. **79** (2008)

[21] S. Etaki, M. Poot, I. Mahboob, K. Onomitsu, H. Yamaguchi, and H. S. J. van der Zant, Nat. Phys. **4**, 785 (2008)

[22] W. Wernsdorfer, Supercond. Sci. Technol. **22**, 064013 (2009)

[23] T. Matsumoto, H. Kashiwaya, H. Shibata, H. Takayanagi, S. Nomura, and S. Kashiwaya, Physica C **471**, 1246 (2011)

[24] D. Vasyukov, Y. Anahory, L. Embon, D. Halbertal, J. Cuppens, L. Neeman, A. Finkler, Y. Segev, Y. Myasoedov, M. L. Rappaport, M. E. Huber, and E. Zeldov, Nat. Nano. **9**, 639 (2013)

[25] D. C. Cox, J. C. Gallop, and L. Hao, Nanofabrication **1**, 53 (2014)

[26] M. Tinkham, *Introduction to superconductivity, 2nd ed.* (McGraw-Hill, 1996)

[27] L. F. Chibotaru, A. Ceulemans, V. Bruyndoncx, and V. V. Moshchalkov, Nature **408**, 833 (2000)

[28] T. Mertelj and V. V. Kabanov, Phys. Rev. B **67**, 134527 (2003)

[29] Y. Mawatari and S. Kashiwaya, private communications. Supplementary data are available online.